THE JOURNAL OF PHYSICAL CHEMISTRY C

Article

Structure and Enhanced Reactivity of Chromocene Carbonyl Confined inside Cavities of NaY Zeolite

Jane Estephane, Elena Groppo, Alessandro Damin, Jenny G. Vitillo, Diego Gianolio, Carlo Lamberti, Silvia Bordiga, Carmelo Prestipino, Sergej Nikitenko, Elsje Alessandra Quadrelli, Mostafa Taoufik, Jean Marie Basset, and Adriano Zecchina

J. Phys. Chem. C, **2009**, 113 (17), 7305-7315• DOI: 10.1021/jp811240m • Publication Date (Web): 03 April 2009

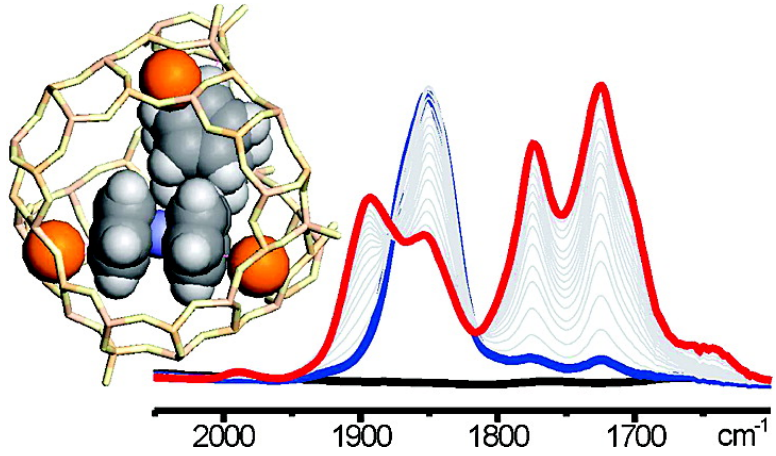

More About This Article

Additional resources and features associated with this article are available within the HTML version:

- Supporting Information
- Access to high resolution figures
- Links to articles and content related to this article
- Copyright permission to reproduce figures and/or text from this article

View the Full Text HTML

Structure and Enhanced Reactivity of Chromocene Carbonyl Confined inside Cavities of NaY Zeolite

Jane Estephane,[†,‡] Elena Groppo,*[,†] Alessandro Damin,[†] Jenny G. Vitillo,[†] Diego Gianolio,[†] Carlo Lamberti,[†] Silvia Bordiga,[†] Carmelo Prestipino,[§] Sergej Nikitenko,[||] Elsje Alessandra Quadrelli,[‡] Mostafa Taoufik,[‡] Jean Marie Basset,[‡] and Adriano Zecchina[†]

Department of Inorganic, Physical and Materials Chemistry, NIS Centre of Excellence and INSTM Centro di Riferimento, University of Turin, Via P. Giuria 7, I-10125 Torino, Italy, Laboratoire de Chimie Organométallique de Surface, UMR5265 "LC2P2", CNRS UCBL1 CPE, 43 Boulevard du 11 Novembre 1918, BP2077, F-69616 Villeurbanne Cedex, France, ESRF, 6 rue Jules Horowitz, BP220, F-38043 Grenoble Cedex, France, and Netherlands Organization for Scientific Research (NWO), DUBBLE @ ESRF, BP 220, 38043 Grenoble Cedex 9, France

Received: December 19, 2008; Revised Manuscript Received: January 16, 2009

Chromocene (Cp_2Cr) hosted inside the supercage cavities of a NaY zeolite undergoes a structural distortion induced by the strong local electric fields generated by charge-balancing counterions. This effect, clearly observed by an in situ Cr K-edge extended X-ray absorption fine structure (EXAFS) study, is the key factor in enhancing the reactivity of Cp_2Cr toward CO. The $Cp_2Cr(CO)$ adducts initially formed are not as stable as when hosted in nonpolar environments such as toluene solution or polystyrene. The presence of strong anionic/cationic pairs (Y^-/Na^+) favors, in a CO atmosphere, the loss of a Cp ring driven by an electron transfer mechanism (accompanied by ligand rearrangement) that results in the formation of the charged $[CpCr(CO)_3]^-$ and $[Cp_2Cr(CO)]^+$ carbonyl species that are stabilized by Na^+ and Y^- pairs. Shape selectivity of the supercage cavity of the Y zeolite is necessary for this reaction, as it can host the two Cp_2Cr molecules needed for disproportionation. Fast Fourier transform infrared (FTIR) spectroscopy, working in operando conditions, allows us to follow the time evolution of the IR stretching modes peculiar of reactants and products and thus to infer a reaction mechanism. The combination of quantum mechanical calculation with an in situ EXAFS study supports the hypothesis made on the basis of IR results. The work is further demonstration that zeolitic voids act as "nanoscale reaction chambers", where the reactivity of guest organometallic complexes can provide molecular insights into the elementary steps of heterogeneous catalysis. In this context, the investigation of metallocene reactivity inside a polar matrix can be extremely useful to understanding their properties in polymerization conditions, where they are usually found as part of an ion pair, together with the anionic form of the activator (e.g., MAO).

1. Introduction

The inclusion of organometallic complexes inside cavities of zeolitic host frameworks is a topic that has gained considerable attention since the 1990s because of the possible applications in heterogeneous catalysis or electronic devices and optical materials[1−7] and because it provides a method for metal incorporation and catalyst immobilization[8,9] inside nanoporous scaffolds, which is an alternative to classical methods such as ion exchange, ligand exchange, and ship-in-the-bottle synthesis.[10−17] The organometallic guests in zeolite hosts become polarized by electrostatic fields resulting from the interplay between positively charged extra-framework cations and negatively charged zeolite walls and are expected to show substantially enhanced reactivity compared to the parent compounds.[18] Therefore, as demonstrated in the past,[18] zeolitic voids would function as "nanoscale reaction chambers", where the reactivity of guest organometallic complexes can provide molecular insights into the elementary steps of heterogeneous catalysis.[18]

Metallocenes are organometallic substrates used to investigate potential reactivity enhancement. Besides undergoing a well-known variety of thermal and photochemical reactions ([2+2] additions and eliminations, oxidative addition and reductive elimination of small molecules, and C−H bond activation),[19,20] they are efficient olefin polymerization catalysts.[21−24] Therefore, the investigation of their reactivity inside a polar matrix can be extremely useful to understand their properties in polymerization conditions, where they are usually found as part of an ion pair, together with the anionic form of the activator (e.g., MAO). Among metallocenes, chromocene, which is the precursor of the Union Carbide olefin polymerization catalyst,[25,26] is a challenging candidate because the study of its reactivity is complicated by electronic spin-pairing effects[27,28] and Cp loss.[19,20,29]

In a previous work,[30] we have already demonstrated that chromocene can be molecularly dispersed inside a polystyrene nanoporous matrix acting as a "solid solvent", allowing spectroscopic and microcalorimetric investigation of the CO coordination process. The nonpolar environment provided by the polystyrene (PS) matrix behaves in a similar way with respect to common solvents,[27,28] and a pressure-dependent $Cp_2Cr + CO \leftrightarrows Cp_2Cr(CO)$ equilibrium is established in the presence of CO.

* Corresponding author. E-mail: elena.groppo@unito.it. Telephone: +39 011 670 7841. Fax: +39 011 670 7855.
[†] University of Turin.
[‡] CNRS.
[§] ESRF.
[||] NWO.

10.1021/jp811240m CCC: $40.75
Published on Web 04/03/2009

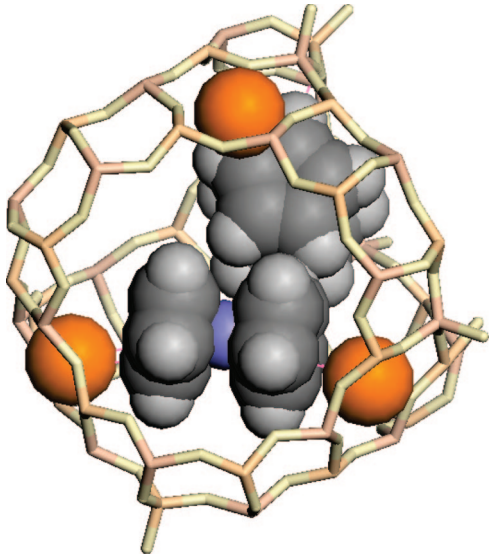

Figure 1. Portion of the faujasite cell, showing the framework and positions of exchangeable Na^+ cations in the SII position within the lattice of the Y zeolite, containing two Cp_2Cr molecules. Framework atoms are represented in the stick mode (Si and Al, light orange; O, light yellow). Na^+ cations and Cp_2Cr molecules are reported as Corey−Pauling−Koltun (CPK) spheres (orange, violet, dark gray, and light gray for Na, Cr, C and H atoms, respectively).

In this paper, we report the encapsulation of chromocene in a NaY zeolite and its reactivity toward CO. The NaY zeolite is chosen because it is characterized by the presence of large internal cavities (supercages) able to host the guest chromocene,[18] thus allowing its easy dispersion without the occurrence of a grafting reaction by covalent bonds (absence of external hydroxyl groups typical of the silica support in the Union Carbide olefin polymerization catalyst). The well-defined dimensions of the supercages circumvent the clustering process that complicates the investigation of the real catalyst. Experimental results based on several complementary techniques (FTIR, UV−vis, XANES, and EXAFS) are supported by theoretical calculations and by comparison with literature data on the optical and vibrational properties of different CO-free MCp_2 (M = Cr, Fe, and Co) systems in a wide range of ion-exchanged Y zeolites.[18] This combined approach allows us to demonstrate the active role played by the NaY electric field[31,32] and the supercage structure in determining the high reactivity of Cp_2Cr toward CO and the chemical nature of encapsulated organometallic fragments.

2. Experimental Section

2.1. Sample Preparation and Experimental Setup. Chromocene (Cp_2Cr, Strem Chemicals, sublimed) was purified by sublimation at 315 K in vacuo. The NaY zeolite (Aldrich) presents a Si/Al ratio of 2.7 and is characterized by the almost total absence of external OH groups (vide infra Figure 4a), a fact that guarantees Cp_2Cr will not undergo a grafting process like that occurring on the silica surface.[25,26,33] The Cp_2Cr/NaY system was obtained by subliming Cp_2Cr inside the cavities of the NaY zeolite previously outgassed at 450 °C for 2 h. This procedure allows us to completely fill the internal cavities of the zeolite. Excess Cp_2Cr adsorbed on the external surface was removed by outgassing at room temperature. The final Cr loading, evaluated from the edge-jump of the extended X-ray absorption fine structure (EXAFS) signal in transmission mode, was around 1 wt %.

For the FTIR spectra of the Cp_2Cr/NaY system, the NaY powder was pressed into a self-supported pellet and then transferred inside an IR cell designed to allow measurements under vacuum or in the presence of a desired equilibrium pressure of gases in the 1000−77 K range. FTIR spectra were collected on a Bruker IFS66 instrument, equipped with a MCT detector, at a resolution of 2 cm^{-1}. For diffuse reflectance spectroscopy (DRS) UV−vis experiments, Cp_2Cr was sublimed directly onto the activated NaY powder inside a UV−vis cell equipped with optical quartz windows. UV−vis spectra were collected on a PerkinElmer Lambda 19 spectrophotometer, equipped with a reflectance sphere.

X-ray absorption experiments at the Cr K-edge (5989 eV) were performed at the BM26A beamline (Dubble) of the ESRF facility (Grenoble, France). The white beam was monochromatized using a Si(111) double crystal; harmonic rejection has been performed by using a meridionally focusing mirror with an angle of incidence of 2.8 mrad and a silicon coating. Because of Cp_2Cr dilution, EXAFS spectra were collected in fluorescence mode, by means of a nine-element germanium monolithic detector. Intensity of the incident beam was monitored by an ionization chamber filled with 1 bar of 20% N_2 and 80% He. The beam transmitted through the sample passed further through a second ionization chamber, a Cr foil, and a third ionization chamber to ensure the correct energy calibration for any acquisition.[34] To avoid contamination of the samples, the Cp_2Cr/toluene reference and the Cp_2Cr/NaY system (in the presence or absence of CO) have been measured inside sealed capillaries (1.5 mm in diameter), following the well-established procedure adopted for X-ray powder diffraction (XRPD) experiments.[35] For this reason, the beam was vertically focused in order to reach a dimension on the sample of 0.3 mm. For each sample, horizontal slits were optimized to fit with the interval of uniform filling of the capillary. The XANES part of the spectra was acquired with an energy step of 0.4 eV and an integration time of 2 s/point. The EXAFS part of the spectra was collected to 12 $Å^{-1}$, with a variable sampling step in energy, resulting in $\Delta k = 0.05$ $Å^{-1}$ and an integration time that linearly increases as a function of k from 5 to 20 s/point to account for the low signal-to-noise ratio at high k values. For each sample, three equivalent EXAFS spectra were acquired and averaged before data analysis.[36]

2.2. Quantum Mechanical Calculations: Computational Details. Quantum mechanical calculations were performed by adopting the Gaussian03 software package.[37] The hybrid density functional theory (DFT) B3LYP functional[38,39] was adopted for the whole series of calculations. Ahlrichs triple zeta valence (TZV) basis set[40] was adopted for Cr atoms, supplemented by one set of Ahlrichs polarization functions. Standard Pople[41] 6-311G(d,p) has been employed for H, C, and O atoms. Spin multiplicity of $2S + 1 = 3$ has been imposed for calculations on bare $CrCp_2$, according to previous experimental[42] and theoretical[30,43] data. The $Cp_2Cr(CO)$, $[Cp_2Cr(CO)]^+$, and $[CpCr(CO)_3]^-$ complexes were computed by adopting $2S + 1 = 1$, $2S + 1 = 2$, and $2S + 1 = 1$ spin multiplicities, respectively. A pruned (99,590) grid has been used for numerical integration in DFT calculations integral (grid = ultrafine in G03). Complexes Cp_2Cr, $Cp_2Cr(CO)$, $[Cp_2Cr(CO)]^+$, and $[CpCr(CO)_3]^-$ have been optimized imposing C_{2v}, C_{2v}, C_s, and C_s symmetry, respectively, and adopting tight thresholds for convergence (opt = tight in G03). For the vibrational features, $\Delta\nu_{CO}$ is obtained according to the following formula: $\Delta\nu_{CO} = \nu_{CO}^{complex} - \nu_{CO}^{bare}$, where $\nu_{CO}^{complex}$ is the computed CO stretching frequency for

TABLE 1: Summary of the Structural Parameters Optimized in Fitting of EXAFS Data for the Cp_2Cr/Toluene, Cp_2Cr/NaY, and Cp_2Cr/NaY + CO Systems[a]

			Cp_2Cr/NaY + CO			
			1 phase	1 phase	2 phases	
	Cp_2Cr/toluene	Cp_2Cr/NaY	$[CpCr(CO)_3]^-$	$[Cp_2Cr(CO)]^+$	$[CpCr(CO)_3]^-$	$[Cp_2Cr(CO)]^+$
S_0^2	0.7 ± 0.1[b]	0.9 ± 0.1	0.9 ± 0.2	0.6 ± 0.1[c]	$0.9x$[d]	$0.9(1-x)$[d]
ΔE_0 (eV)	0 ± 1	-4 ± 2	1 ± 2	1 ± 2	3 ± 1	
$\langle d_{Cr-C} \rangle$ (Å)	2.169 ± 0.006	2.11 ± 0.01	2.193 ± 0.009	2.20 ± 0.01	2.227 ± 0.006	2.196 ± 0.006
σ^2_{Cr-Cp} (Å^2)	0.0032 ± 0.0009	0.010 ± 0.002	0.001 ± 0.001[c]	0.004 ± 0.002	0.0047 ± 0.0006	
$\langle d_{Cr-CO} \rangle$ (Å)	−	−	1.82 ± 0.02	1.85 ± 0.01	1.822 ± 0.006	1.893 ± 0.006
σ^2_{Cr-CO} (Å^2)	−	−	0.012 ± 0.002[c]	0.000 ± 0.001[c]	0.006 ± 0.001	
$n°$ variables	4	4	6	6	6	
R_{factor}	0.020	0.057	0.046	0.035	0.013	

[a] The fits were performed in *R*-space in the 1.0−4.5 Å range over a k^3-weighted FT of the $\chi(k)$ functions performed in the 2.0−10.0 Å^{-1} interval. A single S_0^2 and a single ΔE_0 have been optimized for all SS and MS paths. Parameters not optimized are recognized by the absence of corresponding error bars. [b] The optimized S_0^2 values for $CrCp_2$ molecules in nonpolar media, like toluene or polystyrene, or in the bulk phase are in the 0.6−0.75 range, i.e., significantly lower than the unit value. A value higher and closer to the unit value ($S_0^2 = 0.9 \pm 0.1$) has been obtained when $CrCp_2$ is hosted inside a polar matrix, like the Y zeolite in this work. [c] These optimized values are out of the physical range. Consequently, the one-phase fits are not acceptable (see text for details). [d] The phase fraction parameter *x* is optimized to 0.50 ± 0.007 (see text for details).

each complex, and ν_{CO}^{bare} is the computed CO stretching frequency for the bare molecule.

2.3. XANES and EXAFS Data Analysis. XANES has been simulated using FEFF8.4 code,[44] using the isolated Cp_2Cr molecule with eclipsed geometry as the input cluster, obtained by single crystal diffraction.[42] Calculations for the absorption spectra and densities of states have been done using the muffin-tin potential and Hedin-Lundqvist exchange correlation, taking care of the presence of a core hole in a self-consistency scheme. To take into account the effect of intramolecular vibration in the XANES spectra, the effect of temperature on full multiple scattering is approximated by multiplying each free propagator by $\exp(-k^2\sigma^2)$, where the value of σ^2 is obtained by the fit of the EXAFS[45,46] (Table 1). Although quadrupole transitions are much weaker than the dipole ones, their contribution has been considered in calculations.

EXAFS data analysis was performed using Arthemis software.[47] Phases and amplitudes were calculated with FEFF6.0 code,[48] using as input the structures of Cp_2Cr, $[Cp_2Cr(CO)]^+$, and $[CpCr(CO)_3]^-$ clusters, optimized by quantum mechanical calculations (section 2.2). Phases and amplitudes were successfully verified with Cp_2Cr in toluene solution. For each sample, the averaged $k^3\chi(k)$ function was Fourier transformed in the $\Delta k = 2.0-10.0$ Å^{-1} interval. Fits were performed in *R*-space in the $\Delta R = 1.0-4.5$ Å range (number of independent points, $2\Delta k\Delta R/\pi > 17$).

In the EXAFS data analysis of the Cp_2Cr molecule, the following signals have been considered: (i) 10 Cr−C single-scattering (SS) paths, and (ii) several triangular multiple-scattering (MS) paths, involving two C atoms belonging to the same Cp ring. Conversely, collinear and triangular multiple-scattering paths involving two C atoms of the two different Cp rings do not contribute as expected. This fact, already evidenced by Natoli et al.[49] for the $FeCp_2$ molecule, is explained by considering the dynamic equilibrium between staggered and eclipsed configurations favored by the very low barrier to internal rotations around the C_5 axis. To limit the number of optimized parameters, the two Cp rings have been considered as rigid units, whose distance from Cr is allowed to change in a symmetric way. In this approximation, only four parameters have been optimized (Table 1): S_0^2 and ΔE_0 (common to all paths); the Cr−Cp plane distance (d_{Cr-Cp}), from which all path variations can be defined in a straightforward geometric way (in Table 1 the correlated average $\langle d_{Cr-Cp} \rangle$ distance is reported); and a unique Cr−C Debye−Waller factor for the SS paths (σ^2_{Cr-Cp}) that propagates to the MS paths, according to the square of the path length. For the $[Cp_2Cr(CO)]^+$ and $[CpCr(CO)_3]^-$ models, two additional parameters have been added: the Cr−CO distance ($\langle d_{Cr-CO} \rangle$) and corresponding Debye−Waller factor (σ^2_{Cr-CO}), by considering the CO molecule as a rigid unit linearly bonded to Cr(II).

3. Results

3.1. Sublimation of Cp_2Cr inside NaY Supercages. ***3.1.1. NaY Structure and Diffusion of Cp_2Cr inside the Zeolite.*** Before we discuss the data concerning the reactivity of zeolite-encapsulated chromocene toward CO, it is useful to firmly establish the diffusion behavior and the spectroscopic features of Cp_2Cr hosted inside NaY. For dehydrated NaY zeolites (Si/Al > 2.4) the Na^+ cations are located in three well-defined sites, pointing inside the supercage (the so-called SII position; see orange spheres in Figure 1) or inside more restricted spaces, like the sodalite cage or the hexagonal prisms (both omitted in Figure 1 for simplicity).[50] Because the molecular dimensions of Cp_2Cr are estimated to be 4.862×5.170 Å (kinetic diameter),[51] it can enter freely only into a 12-membered ring entrance window with a diameter of approximately 8 Å,[50] thus accessing the large cavities (α or supercages, with a diameter of about 13 Å) of the NaY zeolite. The Cp_2Cr molecule can thus interact only with Na^+ cations in the SII position.

On the basis of steric properties, it is difficult to make a precise evaluation of the number of Cp_2Cr molecules that can be hosted in a faujasite cage. For the sake of simplicity, we have considered a single cage. By considering the adopted adsorption procedure, it is reasonable to assume that up to two Cp_2Cr molecules are hosted inside a supercage.[18] A simplified representation of the possible host−guest interaction, taking into account the previous observations, is shown in Figure 1. Two Cp_2Cr molecules were placed inside the NaY supercage, with an interaction geometry similar to that found in the case of $FeCp_2$ encapsulated inside NaY.[5] In that case, X-ray and neutron diffraction reveal that, in the presence of $FeCp_2$, the Na^+ cations are shifted toward the center of the supercage, suggesting an interaction between these ions and the Cp rings of the $FeCp_2$ molecule.[5]

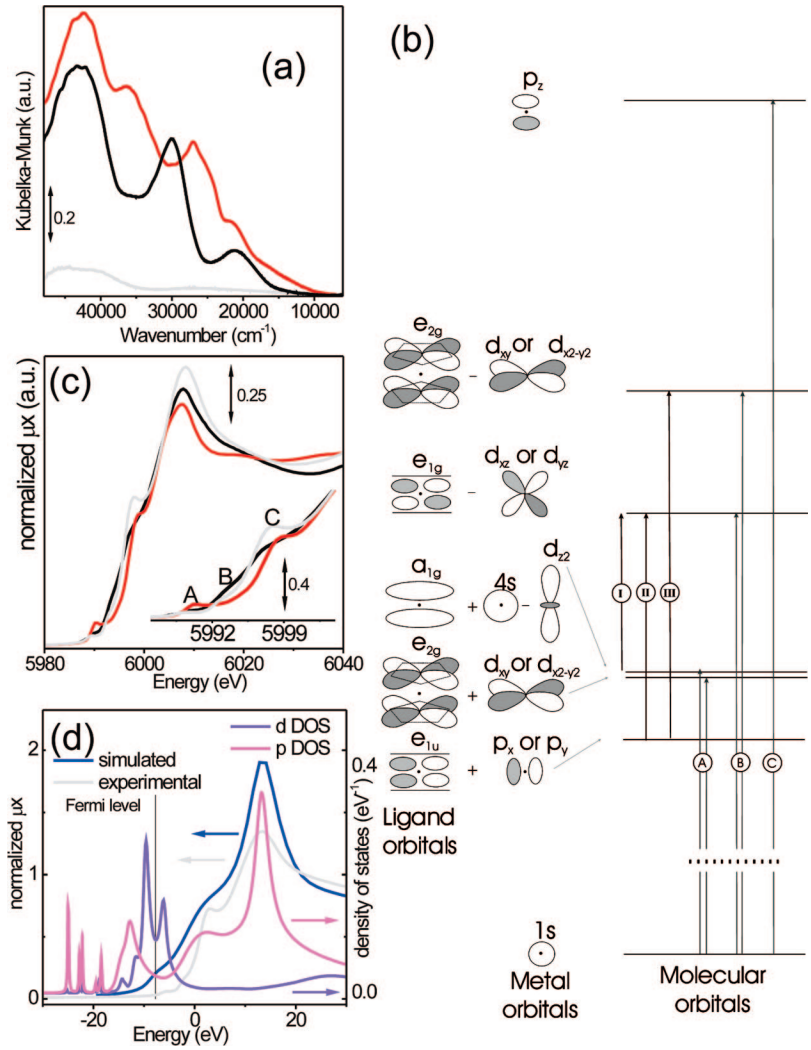

Figure 2. (a) UV−vis DRS spectra of Cp_2Cr/NaY before (black line) and after (red line) CO dosage (equilibrium pressure $P_{CO} = 150$ Torr). The spectrum of the NaY zeolite (gray line) is reported for comparison. (b) Rough representation of the electronic transitions and molecular orbitals involved in the electronic transitions responsible for the UV−vis and XANES spectra. (c) XANES spectra of Cp_2Cr/NaY before (black line) and after (red line) CO dosage (equilibrium pressure $P_{CO} = 150$ Torr). The spectrum of Cp_2Cr in toluene is reported for comparison (light gray). The inset reports a magnification of the pre-edge region. (d) Left ordinate axis shows the simulated XANES spectrum of Cp_2Cr (blue) compared to the experimental spectrum for Cp_2Cr in toluene (light gray, horizontally translated to match the white line position). Right ordinate axis (as indicated by arrows) shows the p- and d-projected density of states (DOS) for the Cr atom (magenta and violet, respectively).

3.1.2. Electronic Properties of Hosted Cp_2Cr: UV−Vis and XANES Results. When Cp_2Cr is sublimed onto the NaY powder, white zeolite acquires a light salmon color. As a consequence, the UV−vis spectrum of the Cp_2Cr/NaY system (Figure 2a, black curve) is characterized by three main components centered around 21000, 30000 (responsible for the color), and 43000 cm^{-1} (henceforth labeled as components I, II, and III, respectively). These bands are very similar to those observed in the spectrum of chromocene in solution.[18,52] In order to assign electronic transitions, one should in principle know the electronic structure of the Cp_2Cr molecule in terms of molecular orbitals. A detailed scheme of the orbital diagram for Cp_2Cr obtained from quantum mechanical calculations, as well as its representation, is beyond the scope of this work. As a first approximation, a simplified scheme constructed on the basis of the well-known diagram valid for the parent $FeCp_2$ system[53,54] is shown in Figure 2b. In the idealized D_{5d} symmetry, the 10 π orbitals of the two Cp rings form the symmetry adapted combinations a_{1g}, a_{2u}, e_{1g}, e_{1u}, e_{2g}, and e_{2u}. Interaction of these ligand-centered orbitals with the metal 3d, 4s, and 4p valence atomic orbitals of appropriate symmetry generates the molecular orbitals shown on the right in Figure 2b.

It is well-known that the Cp_2Cr ground state is $^3E_{2g}$, resulting from the $e_{2g}^3\ a_{1g}^1$ configuration.[52] The transition of one of the 16 valence electrons into a nonoccupied molecular orbital is responsible for the observed optical spectrum. Only the lowest frequency component (21000 cm^{-1}) has been definitely assigned in the literature in terms of a d-d transition ($^3E_{2g} \rightarrow {}^3E_{1g}$, $^3E_{2g}$, $^3A_{1g}$, and $^3A_{2g}$). On the basis of this, band I is due to an electronic transition from the highest-occupied molecular orbital (HOMO) to the lowest-unoccupied molecular orbital (LUMO).[55−57] The d-d character of transition I is easily explained by considering that the HOMO and the LUMO are primarily metal in character (d_{xy,x^2-y^2} for the HOMO and $d_{xz,yz}$ for the LUMO).[58] Conversely, the assignment of the 30000 and 43000 cm^{-1} bands in terms of a crystal field is less straightforward. A tentative interpretation, based on symmetry and energetic considerations, is represented in Figure 2b, according to which both transitions can be classified as ligand-to-metal charge transfer transitions. The key feature from this investigation is that the UV−vis spectrum of Cp_2Cr/NaY clearly indicates that Cp_2Cr is simply encapsulated as a neutral Cp_2Cr molecule inside the supercages of the NaY zeolite, and no further reaction occurs because

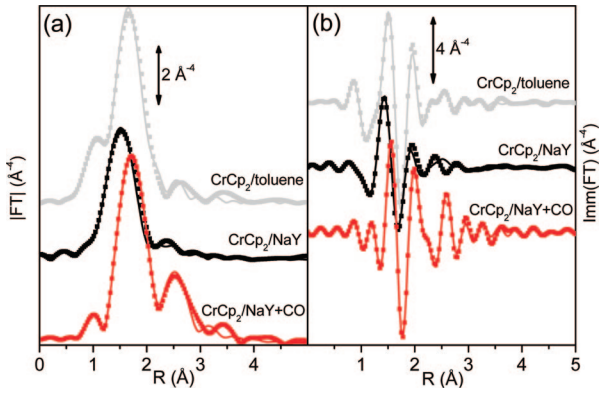

Figure 3. Modulus (a) and imaginary parts (b) of the k^3-weighted, phase-uncorrected Fourier transforms of the EXAFS signal for Cp_2Cr in toluene (top curves, gray), Cp_2Cr hosted in NaY (middle curves, black), and Cp_2Cr hosted in NaY after reaction with CO (bottom curves, red). Experimental data (square dots) are superimposed to the best fit (full lines). For the Cp_2Cr/NaY system, the fit refers to the two phase analysis reported in the last two columns of Table 1.

similar spectra have already been reported for chromocene in solution[18,52] and in a frozen argon matrix.[59]

The same simplified scheme is also useful in understanding the Cr K-edge-normalized XANES spectrum of Cp_2Cr, in the approximation where the core hole generated by the X-ray absorption does not strongly perturb the molecular levels.[60] The XANES spectrum of Cp_2Cr in the NaY zeolite (black curve in Figure 2c) is compared to that of Cp_2Cr in toluene solution (solid gray curve). It is worth noticing that, to the best of our knowledge, a detailed assignment of the XANES spectrum of Cp_2Cr (either solid or in solution) has never been reported, while descriptions of the XANES spectra of the parent Cp_2Fe and Cp_2Ni systems[7,49] and of other Cr-based organometallic complexes[61,62] can be found in literature.

The spectrum of the reference sample is characterized by three main features in the pre-edge region at 5989.2, 5992.8, and 5997.7 eV (labeled A, B, and C, respectively), followed by an intense and sharp white line centered at 6008.2 eV (Figure 2c). For assignment of these features, we have performed a simulation of the XANES spectrum of the Cp_2Cr molecule with FEFF8.4 code,[44] as previously described in section 2.3. Figure 2d compares the simulated XANES spectrum of the isolated molecule (blue) with that of the experimental molecule collected in a toluene solution (light gray), which was properly translated to match the energy position of the white line transition. The simulated spectrum is in good agreement with the experimental spectrum and is able to reproduce the energy position and relative intensity of all the features. The differences between the simulated and experimental spectra consist only of: (i) a systematic overestimation of the feature's intensity, compared to the edge jump, and (ii) a systematic small overestimation of the broadness of the features. The calculated projected DOS for the Cr atom is also shown on the same energy scale in Figure 2d (right ordinate axis). Comparison of the simulated spectrum with the projected DOS allows the assignment of the main XANES features that can be divided in two families. At lower energy, features A and B are due to the transition between the 1s orbital and Cr levels characterized by a significant p/d hybridization. At higher energy, C and white line features are due to the transition of a 1s electron into almost "pure" p levels. On the basis of this simulation, the intense feature C is assigned to the dipole-allowed $1s \rightarrow 4p_z$ transition (see the electronic scheme reported in Figure 2b) and is consequently very sensitive to coordination and geometric variation along the z axis of the molecule.[49] For a complete assignment of features A and B, a combination of XANES (Figure 2c) and UV−vis (Figure 2a) spectra is mandatory. The energy difference between the levels originating from the $e_{1g}-d_{xz},d_{yz}$ (LUMO) and $e_{2g}-d_{xy},d_{x^2-y^2}$ antibonding combinations is 13000 cm^{-1} (1.6 eV), from the UV−vis spectrum (frequency difference between band III and band II), which is a value too narrow to be resolved in the XANES spectrum because of core-hole broadening. Shoulder B is consequently assigned to the unresolved electronic transitions from 1s to these levels. Finally, feature A, found 3.6 eV (29000 cm^{-1}) below B, is assigned to the dipole-forbidden transitions from the 1s to the HOMO levels. In fact, the UV−vis spectrum reveals that the almost degenerated and partially unoccupied HOMO levels lie 21000 cm^{-1} below the LUMO levels and 34000 cm^{-1} below the levels originated from the $e_{2g}-d_{xy},d_{x^2-y^2}$ antibonding combinations, respectively (average value is 27500 cm^{-1}, as XANES does not resolve the two final states).

The XANES spectrum of the Cp_2Cr/NaY system presents basically the same main features discussed so far for Cp_2Cr in toluene, corroborating the conclusion of the UV−vis study, i.e., that Cp_2Cr is confined in the NaY supercages without changes in the Cr oxidation state. However, the spectrum is less resolved, indicating a higher heterogeneity of the species. This is assigned to different local electric fields experienced by Cp_2Cr molecules due to different statistical cation distribution in the supercages (Figure 1). In further detail, feature A remains basically unchanged and feature B increases in intensity, while an inverse behavior is observed for feature C and the white line. Because the most affected feature is feature C, we expect an appreciable structural modification of the Cp_2Cr molecule along the z axis due to interaction with the zeolitic walls and to the presence of strong local electric fields[31,32] (see the EXAFS analysis in section 3.1.3).

3.1.3. Structural and Vibrational Properties of Hosted Cp_2Cr: EXAFS and FTIR Results. Figure 3 shows the k^3-weighted, phase-uncorrected Fourier transform (FT) of the EXAFS signal for Cp_2Cr molecule in toluene (top curves, gray) and hosted in NaY (middle curves, black). Encapsulation in NaY results in an evident shortening of the first shell peak (due to the SS of the C atoms of the Cp rings) and the higher R contribution (due to the triangular MS paths), reflecting a contraction of the Cr−Cp distance with respect to the molecule in solution. This is confirmed by data analysis, reported in Table 1, quantifying a contraction of the average Cr−C distance of 0.06 Å. This is the main origin of the structural modification of the molecule along the z axis that has been observed in the XANES study (Figure 2c).

Also, Cp_2Cr/NaY exhibits a first shell peak less intense and broader than that of the molecule in solution. Data analysis indicates that this behavior is caused by increased heterogeneity, quantified by the Debye−Waller factor (σ^2) that increases from 0.003 to 0.010 Å^2 (Table 1). The σ^2 value of 0.010 Å^2, measured for the Cp_2Cr/NaY system, has consequently a main static origin and agrees with the broadening of the pre-edge XANES features (Figure 2c). This heterogeneity is also responsible for the lower quality of the fit for the Cp_2Cr/NaY system with respect to Cp_2Cr in solution (see R_{factor} in Table 1 and compare full and dotted curves in Figure 3 for the two systems).

Figure 4a shows the FTIR spectrum of the NaY zeolite before (gray curve) and after (black curve) Cp_2Cr sublimation. Note the extreme weakness of the ν(OH) bands (around 3700 cm^{-1}), testifying the almost complete absence of Si-OH groups that are left unchanged after Cp_2Cr sublimation. Upon Cp_2Cr dosage,

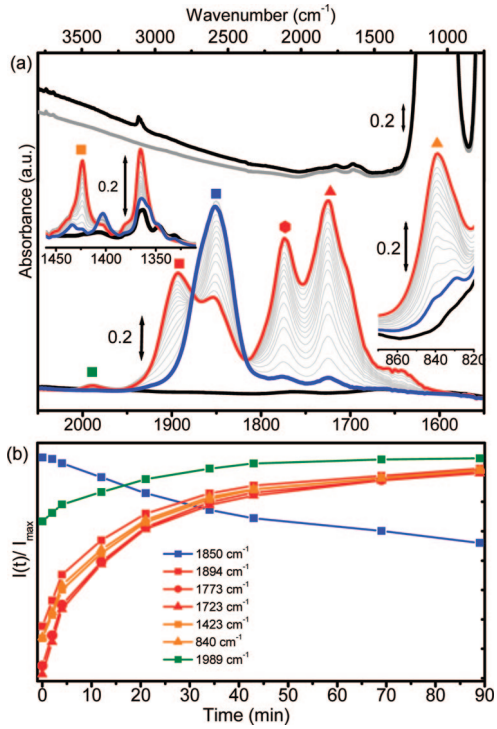

Figure 4. (a) Top: FTIR spectra of the NaY zeolite before (gray line) and after (black line) Cp_2Cr sublimation. Central: Time evolution at room temperature of the FTIR spectra (background subtracted) of the Cp_2Cr/NaY system after contact with CO (equilibrium pressure P_{CO} = 150 Torr). Blue curve: Immediately after CO dosage inside the cell. Red curve: After 1 h from CO dosage inside the cell. Gray curve: Intermediate times. Left and right insets report the υ(C═C) and υ(CH) stretching regions, while the central portion reports the υ(CO) stretching region. (b) Kinetics of consumption of the precursor/formation of the products, as evaluated from the decrease/increase in intensities (normalized to I_{max}) of the corresponding IR bands.

we observe the appearance of weak components around 3107 and 1364 cm^{-1} (Figure 4a top and left inset) that can be roughly assigned to the υ(C−H) and υ(C═C) stretching modes of the hosted Cp_2Cr molecule, respectively. Unfortunately, the most intense vibrational modes of Cp_2Cr, occurring at 1090, 990, and 770 cm^{-1},[30,63−65] are not visible because they are obscured by the intense vibrational features of the zeolite framework. Once the Cp_2Cr diffusion through the zeolite cages has been completed, the FTIR spectrum does not evolve with time, confirming that the cavities are completely filled and, once again, that Cp_2Cr is simply encapsulated as a neutral molecule inside the NaY supercages; no further reactions occur.

3.2. Reactivity of Cp_2Cr/NaY toward CO. ***3.2.1. In Situ Investigation Using FTIR Spectroscopy of the First Steps of the Reaction.*** Upon addition of CO to $CrCp_2$/NaY [P(CO) = 150 Torr at room temperature], an intense band in the υ(CO) region at 1850 cm^{-1} immediately appears (blue curve in Figure 4a), which is assigned to the 18-electron monocarbonyl complex of type [Cp_2Cr(CO)]. The υ(CO) band of [Cp_2Cr(CO)]/NaY is red shifted by about 50 cm^{-1} with respect to the [Cp_2Cr(CO)] adduct formed in toluene solution[27] and inside the polystyrene matrix[30] (in both cases υ(CO) = 1900 cm^{-1}). We attribute such a red shift to the interaction of the [Cp_2Cr(CO)] complex with the highly ionic environment of the zeolite cavities and in particular with the Na^+ cations. Analogous experiments conducted on K^+-, Mg^{2+}-, and Ca^{2+}-substituted Y zeolites gave the same [Cp_2Cr(CO)] complex characterized by υ(CO) = 1864, 1840, and 1836 cm^{-1}, respectively (data not shown). The frequency shift with respect to the [Cp_2Cr(CO)] species in the polystyrene neutral environment [υ(CO) = −36, −50, −60, and −64 cm^{-1} for K^+, Na^+, Mg^{2+} and Ca^{2+}, respectively] is substantially in agreement with the polarizing ability of the different cations.[66]

While the [Cp_2Cr(CO)] adduct formed inside the polystyrene matrix is stable at room temperature,[30] the spectrum of [Cp_2Cr(CO)] encapsulated in NaY undergoes a rapid evolution over time (from the blue to red spectra in Figure 4a). The major phenomenon appears in the υ(CO) region (Figure 4a, central), where the band at 1850 cm^{-1} is progressively eroded, with the simultaneous appearance of three bands at 1893, 1773, and 1724 cm^{-1} (red symbols) accompanied by two isosbestic points at 1877 and 1816 cm^{-1}. Minor features are the appearance of a weak component at ∼1980 cm^{-1} (green squares) and of complex absorptions in the 1450−1350 cm^{-1} (left inset, Figure 4a) and 950−800 cm^{-1} (right inset, Figure 4a) regions that will be further discussed. The evolution of the FTIR spectra in the ν(CO) region suggests that the main phenomenon occurring with time is the transformation of the monocarbonyl Cp_2Cr(CO) precursor (blue curve, Figure 4) into a tricarbonyl species of type $CpCr(CO)_3$ (red curve, Figure 4), characterized by a symmetry lower than C_{3v}. The kinetics of the process have been estimated by monitoring the decrease/increase of each FTIR band as a function of time (Figure 4b). The theoretical calculations (section 3.2.2) and comparison with the υ(CO) values reported in the literature for the $[CpCr(CO)_3]^-Na^+$ homogeneous complex in solution in perfect C_{3v} symmetry (2 bands at 1880 and 1695 cm^{-1}, baricenter at 1787 cm^{-1})[67] indicate that the $CpCr(CO)_3$ fragment is anionic. The presence of three bands instead of two is due to removal of degeneracy caused by the interaction with Na^+ cations. Conversely, the cationic $[CpCr(CO)_3]^+$ species are not compatible with the observed $\tilde{\upsilon}$(CO).[68] The previous assignment implies a fast release of a Cp ligand from the Cp_2Cr(CO) precursor to the NaY system, as is discussed in section 4.

The formation of the $[CpCr(CO)_3]^-$ anionic complex is accompanied by other phenomena, as shown by the appearance of several other components in the FTIR spectra shown in Figure 4a. In particular, the couple of bands at 1423 and 1365 cm^{-1} (left inset, Figure 4a) and the complex absorption centered at 840 cm^{-1} grow following the same kinetics of the bands associated with the $[CpCr(CO)_3]^-$ anionic complex (red and orange curves, Figure 4b), suggesting that they belong to the same species. A weak component grows faster with time (green curve, Figure 4b) in the υ(CO) region at ∼1980 cm^{-1} (i.e., ∼130 cm^{-1} higher than the band due to the neutral Cp_2Cr(CO) precursor). This band can be assigned to a fraction of $[Cp_2Cr(CO)]^+$ species. Indeed, a similar increase in υ(CO) has been recently reported for an ansa-bridged chromocene carbonyl cation formed by one-electron oxidation of the neutral Cp_2Cr carbonyl species by a Brønsted acid.[69] Note that no conclusions can be drawn for the concentration of the cationic species from the intensity of the band at ∼1980 cm^{-1}, because of the lower extinction coefficient expected for carbonyls giving absorption in this frequency range.[70]

The previous assignments of the FTIR spectra, in terms of the copresence of the anionic $[CpCr(CO)_3]^-$ and cationic $[Cp_2Cr(CO)]^+$ species, are further confirmed by the evolution of the spectra upon dosing NH_3 (Figure 5). The original three-band carbonylic spectrum becomes more resolved and is transformed into a two-band spectrum, with main components at 1890 and 1765 cm^{-1}. The broad band appearing around 1630 cm^{-1} is due to the bending mode of the liquid-like NH_3 physisorbed in the zeolitic cavities.[71,72] NH_3 coordination is

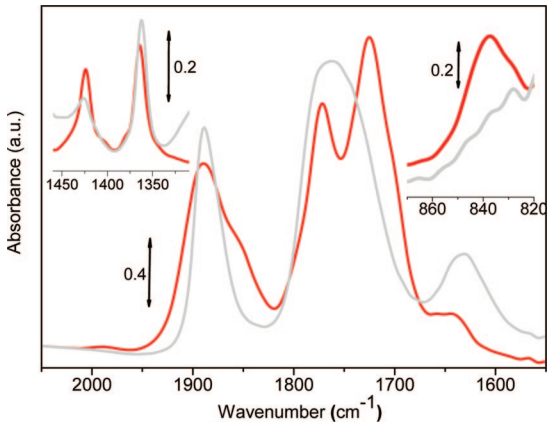

Figure 5. Effect of NH_3 dosage (equilibrium pressure $P_{NH_3} = 150$ Torr) on the Cp_2Cr/NaY system after reaction with CO (equilibrium pressure $P_{CO} = 150$ Torr). Red curve: After 1 h from CO dosage inside the cell. Gray curve: Dosage of NH_3.

TABLE 2: Geometrical Features of $CrCp_2$, $[CrCp_2(CO)]^+$, and $[CrCp(CO)_3]^-$ As Obtained from Theoretical Calculations[a]

	$CrCp_2$	$[CrCp_2(CO)]^+$	$[CrCp(CO)_3]^-$
$Cr-C_{Cp}$ (Å)	2.138	2.238	2.255
	2.179	2.216	2.266
	2.179	2.244	2.266
	2.247	2.216	2.259
	2.247	2.382	2.259
$\langle Cr-C_{Cp}\rangle$ (Å)	2.198	2.259	2.261
X−Cr−X (deg)	178.5	148.2	−
$Cr-C_{CO}$ (Å)	−	1.893	1.822

[a] $Cr-C_{Cp}$ and $\langle Cr-C_{Cp}\rangle$ are the distances and the average distance, respectively, between the Cr and C atoms of Cp. X−Cr−X values are the angles formed by the center of mass of the two Cp rings and the Cr atom. $Cr-C_{CO}$ is the distance between Cr and the C atom of the CO molecule.

completely reversible upon desorption at room temperature, with consequent restoration of the tricarbonyl original bands (spectra not shown). This process is commonly observed in solution when the $[CpCr(CO)_3]^-M^+$ species is in contact with a Lewis base[73,74] and can be explained with the transformation of the original tight contact pair $[Cp_2Cr(CO)]^+Y^-$ and $Na^+[CpCr(CO)_3]^-$ into a separated ion pair ($[Cp_2Cr(CO)]^+NH_3$ $[CpCr(CO)_3]^-$), where the $[CpCr(CO)_3]^-$ species assumes a local C_{3v} symmetry. The solvating effect of NH_3 toward the charged carbonylic species is confirmed by the strong perturbation of other vibrational modes assigned to the $[CpCr(CO)_3]^-$ group; in particular, the intense band at 840 cm^{-1} is almost completely eroded. The complete reversible behavior upon NH_3 adsorption/desorption clearly demonstrates that the observed phenomenon is a simple coordination, and no destruction of the $[CpCr(CO)_3]^-$ and $[Cp_2Cr(CO)]^+$ complexes occurs. A similar phenomenon has been already observed in the past for the anionic carbonyl species on different oxidic surfaces.[75,76]

3.2.2. Quantum Mechanical Calculated Vibrational Features and Geometric Details. Quantum mechanical calculations were performed on neutral $Cp_2Cr(CO)$ and on the charged $[Cp_2Cr(CO)]^+$, $[CpCr(CO)_3]^-$, and $[CpCr(CO)_3]^+$ complexes in order to further confirm the assignment of the vibrational features previously discussed. Geometrical details of the optimized structures are reported in Table 2, while theoretical $\Delta\nu_{CO}$ values are compared to experimental values in Table 3. The direction and extent of the shifts observed experimentally are very satisfactorily modeled for the $Cp_2Cr(CO)$, $[Cp_2Cr(CO)]^+$, and $[CpCr(CO)_3]^-$ complexes (corresponding computed IR spectra are reported in Figure S1 of the Supporting Information), while the $\Delta\nu_{CO}$ calculated for the cationic $[CpCr(CO)_3]^+$ species is one order of magnitude lower with respect to the experimental values. We can therefore infer that quantum mechanical calculations support the experimental results, and our previous assignment in terms of the copresence of anionic $[CpCr(CO)_3]^-$ and cationic $[Cp_2Cr(CO)]^+$ species. Notice that all of the experimental $\Delta\nu_{CO}$ values are ~60 cm^{-1} greater (in absolute value) with respect to the theoretical values, a fact that can be explained by considering the environment provided by the NaY cavities versus the ideal conditions corresponding to theoretical calculations. Note that the computed $\Delta\tilde{\nu}_{CO}$ is in perfect agreement with the experimental value obtained for the $Cp_2Cr(CO)$ complex in neutral polystyrene (−243 cm^{-1}).[30]

3.2.3. Electronic Properties of the Reaction Products: XANES and UV−Vis Results. The UV−vis and XANES spectra of the Cp_2Cr/NaY system, after prolonged interaction with CO (red curves, Figure 2a,c, respectively), are strongly modified with respect to those before CO exposure (black curves, Figure 2a,c). Starting with the UV−vis spectrum, the addition of CO results in the appearance of new absorption bands centered around 16000, 26000, and 35000 cm^{-1} that are overlapped with the original I, II, and III bands. The new components are compatible with the formation of a chromocenium cation, in analogy with the spectrum of the $[Cp_2Cr]^+Cl^-$ complex in acetonitrile reported in the literature (bands at 16000, 25000, and 34000 cm^{-1}).[18]

In the XANES spectrum (red curve in Figure 2c), upon CO addition the white line intensity and pre-edge features are strongly modified. In particular, feature A shifts to 5990.3 eV (almost doubling its intensity) and feature B is strongly depleted, whereas feature C blue shifts at 5998.5 eV. Features A and C are better resolved than those of the Cp_2Cr/NaY system, suggesting a better molecular definition of the Cr species formed upon CO contact. In this regard, it is worth noticing that having no inversion center the $[CpCr(CO)_3]^-$ and $[Cp_2Cr(CO)]^+$ product species hypothesized from the IR study (section 3.2.1) could justify the important increase in intensity of the dipole-forbidden feature A of the XANES spectrum. Conversely, the position of the edge is almost unaltered with respect to the Cp_2Cr/NaY system. In principle, in the $[CpCr(CO)_3]^-$ and $[Cp_2Cr(CO)]^+$ product species, Cr should be characterized by a different formal oxidation state with respect to the starting Cp_2Cr species, unless the negative or positive charges are delocalized across the entire molecule and not localized on the Cr center.

3.2.4. Structural Characterization and Quantitative Evaluation of the Reaction Products: EXAFS Results. FTIR, UV−vis, and XANES spectroscopies, in combination with

TABLE 3: Experimental (obtained in NaY) and Theoretical (obtained with B3-LYP functional) $\Delta\tilde{\nu}_{CO}$ values for Four Carbonyl Complexes

	$Cp_2Cr(CO)$		$[Cp_2Cr(CO)]^+$		$[CpCr(CO)_3]^+$		$[CpCr(CO)_3]^-$	
	experimental	theoretical	experimental	theoretical	experimental	theoretical	experimental	theoretical
$\Delta\tilde{\nu}_{CO}$ (cm^{-1})	−293	−226	−163	−115	−	−71	−419	−336
					−	−62	−370	−336
					−	−10	−250	−250

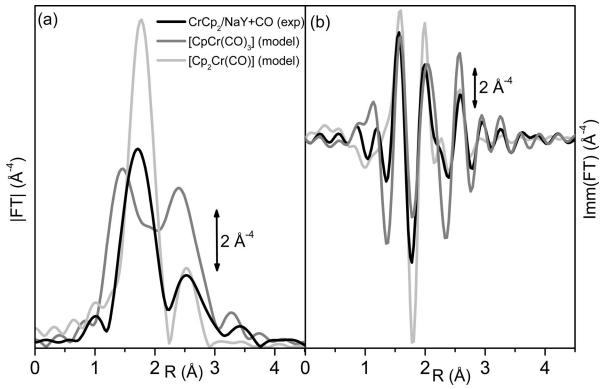

Figure 6. Comparison between the k^3-weighted, phase-uncorrected FT of the Cp_2Cr/NaY system after prolonged interaction with CO (black curves) and the simulated spectra ($\sigma^2 = 0.005$ Å^2, $\Delta E = 0$ eV, and $S_0^2 = 1$) obtained from the optimized structures of the $[CpCr(CO)_3]^-$ (dark gray curves) and $[Cp_2Cr(CO)]^+$ (light gray curves) complexes obtained from quantum mechanical calculations. (a) and (b) refer to the modulus and imaginary parts, respectively. Note that here we report models and not fits.

quantum mechanical calculations, give strong indications about the nature of the products of reaction between the Cp_2Cr/NaY system and CO. A structural characterization and quantitative evaluation of their relative amounts are obtained by the EXAFS study. It is worth recalling that because of moisture sensitivity of the sample, the X-ray absorption spectra were collected on sealed capillaries (section 2.1). Because the time of CO contact in the XAS experiment is much longer than that of the last IR spectrum (red curve, Figure 4a), the initial species $Cp_2Cr(CO)$ is not expected to be detected by EXAFS, while only the final state with the copresence of the $[CpCr(CO)_3]^-$ and $[Cp_2Cr(CO)]^+$ species is expected to be observed.

The experimental k^3-weighted, phase-uncorrected FT spectrum of the Cp_2Cr/NaY system, after prolonged interaction with CO (red square-dotted curve, Figure 3a), exhibits three well-resolved components (distances not corrected in phase): (i) a dominant peak at 1.71 Å, which is due to the interference between the [Cr−C] SS paths from the Cp ring(s) and CO molecule(s); (ii) a component at 2.52 Å, due to the triangular [Cr−C−C] MS paths of the Cp ring(s), the [Cr−O] SS path of the CO molecule(s), and two collinear [Cr−C−O] MS paths of the CO molecule(s); and (iii) a weak contribution centered at 3.44 Å, due to the collinear [Cr−C−O] MS paths of the CO molecule(s), covering the CO molecule length twice back and forth.

EXAFS signals of the $[CpCr(CO)_3]^-$ and $[Cp_2Cr(CO)]^+$ structures optimized by quantum mechanical calculations have been simulated (by arbitrarily defining $\sigma^2 = 0.005$ Å^2, $\Delta E = 0$ eV, and $S_0^2 = 1$, Figure 6).[77] The simulated spectrum for the $[Cp_2Cr(CO)]^+$ model (light gray curves, Figure 6) is characterized by a more intense first shell peak simply because the first shell Cr−C SS contributions for the Cp and CO molecules are more in phase than in the $[CpCr(CO)_3]^-$ model.[78] Similarly, the higher intensity of the second and third peak of the anionic species model (dark gray curves, Figure 6) reflects the higher number of CO molecules. At first, neither model reproduces satisfactorily the experimental data (black curves, Figure 6). Indeed, when the structural parameters are optimized, an acceptable mathematical agreement between experimental and simulated spectra is obtained (see R_{factor} values in Table 1, fit curves are not reported), but some of the optimized variables are out of the physical range. In particular, the model based only on the anionic species $[CpCr(CO)_3]^-$ gives a value of $\sigma^2_{Cr-Cp} = 0.001$ Å^2 (four times less than that of the Cp_2Cr in toluene), suggesting that one Cp ring per Cr atom is not enough to reproduce the experimental data. Analogously, a Debye−Waller factor of the CO molecule greater by one order of magnitude, $\sigma^2_{Cr-CO} = 0.012$ Å^2, clearly indicates that the average number of CO molecules per Cr must be lower than three. Likewise, the model based only on the cation $[Cp_2Cr(CO)]^+$ species leads to physically unacceptable parameters. The amplitude factor of $S_0^2 = 0.59$ is too far from the unit value to be reasonable, while the optimized Debye−Waller factors are inverted, $\sigma^2_{Cr-Cp} = 0.004$ Å^2 and $\sigma^2_{Cr-CO} = 0.000$ Å^2. The combination of the S_0^2 and σ^2 values indicates that on average Cr atoms should have less than two Cp ligands and more than one CO ligand.

Failures of the first two fits confirm that both the $[CpCr(CO)_3]^-$ and $[Cp_2Cr(CO)]^+$ species contribute to the experimental spectrum, which is in agreement with the FTIR results (section 3.2.1). To establish the cation/anion stoichiometry, a two-phase fit was performed. A phase fraction parameter x was added to the fit, weighting the signals of the species $[CpCr(CO)_3]^-$ and $[Cp_2Cr(CO)]^+$ by x and $1 - x$, respectively.[79,80] In order to limit the number of optimized parameters, the amplitude factor was fixed to its optimized value in the Cp_2Cr/NaY system ($S_0^2 = 0.9$, third column in Table 1); also, the same Debye−Waller factors and the same Δd_{Cr-Cp} and Δd_{Cr-CO} parameters were used for the Cp and CO molecules of the two complexes.[81] With this approach, the number of optimized parameters is six, the same as for the two previous fits, so that the values of the R_{factor} can be directly compared among the three fits. The two-phase fit (sixth and seventh column in Table 1) has an $R_{factor} = 0.013$, which is 3.5 and 2.5 times better than those obtained in the previous single-phase fits. More importantly, all optimized parameters lie within the physically acceptable ranges. With the phase fraction parameter x being optimized to 0.50 ± 0.07, we conclude that the two species are almost equi-populated. The quality of the fit is appreciable in Figure 3 (bottom curves) and is further confirmed by the relative value of the correlation among fitted parameters.[82]

Despite the fact that the obtained results are satisfactory, the stability of the two-phases fit reported in Figure 3 and Table 1 must be carefully verified and the presence of other possible local minima accurately discarded. In fact, EXAFS is, in principle, able to identify two (or more) different phases inside the investigated sample and to quantify their relative amounts.[79,80] High accuracy in the quantification is obtained when the two phases are characterized by different ligands around the absorbing atom. Unfortunately, this is not the case for the $[CpCr(CO)_3]^-$ and $[CpCr(CO)]^+$ species, which contain the same ligands (Cp and CO, at slightly different distances) but with different stoichiometries. This problem is particularly evident when considering that both one-phase fits resulted in acceptable R_{factor} values (Table 1), and they have been discarded only on the basis of the nonphysical values of some variables (Debye−Waller factors and S_0^2).

For this reason, the range of validity of the two-phase EXAFS fit has been carefully investigated by fixing the fraction x of the $[CpCr(CO)_3]^-$ species in the 0−1 interval with steps of 0.1 and by performing the 2-phase fit for each x value with the same procedure discussed above. The evolution of the R_{factor} and σ^2_{Cr-Cp} and σ^2_{Cr-CO} as a function of x is reported in panels a and b of Figure 7, respectively. Considering the R_{factor} trend (Figure 7a), it is evident that $x = 0.5$ is a well-behaved absolute minimum for the two-phase fit, and no other relative minima are present. The σ^2_{Cr-Cp} evolution as a function of x is opposite to that of σ^2_{Cr-CO} (Figure 7b). This behavior is definitive proof

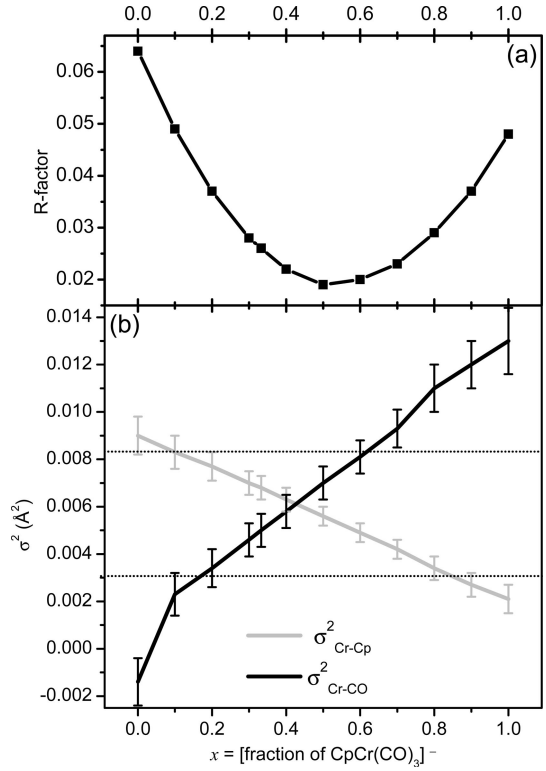

Figure 7. Evolution of R_{factor} (a) and σ^2_{Cr-Cp} and σ^2_{Cr-CO} (b) as a function of the fraction x of the $[CpCr(CO)_3]^-$ species optimized in two-phase fits performed at fixed x values. Horizontal lines in (b) define the upper and lower limits of acceptability of the Debye−Waller factors, set to 0.008 and 0.003 Å^2, respectively. These values were chosen on the basis of our experience for well-defined systems, where the contribution of the static disorder to the Debye−Waller factors is minimal.

that the two phases must be present in a consistent amount. In fact, when to low x values ($[CpCr(CO)_3]^-$ fraction) are imposed, the algorithm tries to increase the contribution of the CO ligands by lowering σ^2_{Cr-CO} below the physically acceptable values and to decrease the contribution of the Cp ligands by increasing σ^2_{Cr-Cp} above the physically acceptable values. The opposite behavior is observed when overly low x values are imposed. By considering the physically meaningful Debye−Waller factors in the 0.003−0.008 Å^2 range (horizontal lines, Figure 7b), x values in the 0.2−0.6 interval can be accepted (note that in this x interval the R_{factor} values are very close to the minimal value).

4. Discussion

When exposed to CO pressure, chromocene yields a monocarbonyl adduct $Cp_2Cr(CO)$, which is indefinitely stable in the solid state inside a nonpolar polystyrene matrix.[30] It is reported that in toluene solution the neutral monocarbonyl complex evolves slowly toward a charged species, among which is $[CpCr(CO)_3]^-$.[83] In this work, we have demonstrated that in a NaY zeolite the monocarbonyl very rapidly evolves to the $[Cp_2Cr(CO)]^+$ $[CpCr(CO)_3]^-$ ion pair, stabilized by the ionic environment provided by the zeolite. The formation of the $[Cp_2Cr(CO)]^+$ $[CpCr(CO)_3]^-$ ion pair implies the occurrence of two processes, simultaneously or successively: (i) a redox process and (ii) the displacement of one Cp ligand. The occurrence of these two processes is based on two important conditions. (1) The Cp rings of the Cp_2Cr molecule are slightly negatively charged; therefore, it seems natural that they orient toward Na^+ cations by electrostatic interactions (Figure 1), as

SCHEME 1: Proposed Reaction Mechanism for Formation of the $[CpCr(CO)]^+$ $[CpCr(CO)_3]^-$ Ion Pair in the NaY Cavity

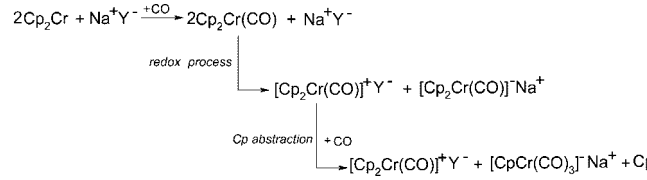

in the case of ferrocene.[5,84,85] These interactions, responsible for the position of the Cp_2Cr molecule found inside the NaY host, could also be the driving forces of the subsequent Cp ligand loss under a CO environment. (2) To take into account the stoichiometry of the process, the simultaneous presence of more than one Cp_2Cr molecule inside the same supercage is necessary. It is worth noticing that intrazeolite photoelectron transfer has been demonstrated to occur through neighboring cages in the presence of large electron donor/acceptor pairs, which cannot fit in the same cages.[86] This situation seems, however, less probable in our case because charge transfer is accompanied by disproportion and ligand transfer, which seem unlikely for nonadjacent molecules.

Because of this, a mechanism guiding the enhanced reactivity of Cp_2Cr/NaY toward CO can be hypothesized (Scheme 1). On the basis of the reported equilibrium constant[27] and the experimental CO pressure (P_{CO} = 150 Torr), it can be estimated that more than 90% of chromocene will have coordinated a CO molecule. From a neutral $Cp_2Cr(CO)$ precursor, a cationic $[Cp_2Cr(CO)]^+$ and transient anionic $[Cp_2Cr(CO)]^-$ species (the latter is not detectable by any technique) are formed by electron transfer, the disproportionation being promoted by the Cp_2Cr distortion[87] induced by the zeolitic electrostatic field. The cation is stabilized by the zeolitic framework and the anion by Na^+. This latter $[Cp_2Cr(CO)]^-$ species undergoes an already observed Cp ring slippage and eventually a Cp ring loss[83] to produce the $[CpCr(CO)_3]^-$ anion. Note that electron transfer can also occur between a neutral monocarbonyl $Cp_2Cr(CO)$ precursor and a fraction of the uncomplexed Cp_2Cr molecule, possibly electronically enriched by the anionic zeolitic framework with the consequent formation of an anionic $[Cp_2Cr(CO)]^-$ and cationic $[Cp_2Cr]^+$ species, the latter in rapid equilibrium with its carbonyl adduct $[Cp_2Cr(CO)]^+$. In summary, the mechanism implies the formation of the $[Cp_2Cr(CO)]^+$ and $[CpCr(CO)_3]^-$ species, whose presence after prolonged contact with CO has been demonstrated by means of all of the adopted techniques and predicts a ratio of $[CpCr(CO)_3]^-$ to $[CpCr(CO)]^+$ of 1:1, which is in agreement with the quantitative evaluation obtained by the EXAFS study (section 3.2.4 and Table 1). In conclusion, it is evident that the electrostatic field present in the zeolite cage plays a determinant role in reactivity enhancement, either as a "stabilizer" of the final ionic products or as an active partner in the electron transfer process, by abstraction of a Cp ring.

5. Conclusions

$Cp_2Cr(CO)$ molecules hosted inside supercages of a NaY zeolite show substantially enhanced reactivity compared to that of the parent compound in a neutral environment. While the $Cp_2Cr(CO)$ adduct is indefinitely stable in PS nanovoids[30] and undergoes a very slow CO decay in solution,[83] such an adduct is not stable in zeolite cavities and undergoes electron transfer and ligand rearrangement to yield the $[CpCr(CO)_3]^-$ and $[CpCr(CO)]^+$ species. This result indicates that, unlike PS

nanovoids, zeolite cavities promote intermolecular reactions between hosted molecules much faster than that of its solution counterpart. In other words, the internal architecture of the zeolite (i.e., presence of high internal electric fields and "coordinatively unsaturated" Na^+ extra-framework cations) offers a unique reaction environment to the encapsulated Cp_2Cr molecules. The simultaneous and synergic combination of different spectroscopic techniques, associated with quantum mechanical theoretical calculations, allow us to fully understand the complex reactivity of Cp_2Cr molecules toward CO inside polar cavities of the NaY host and to advance a reaction mechanism.

Acknowledgment. Financial support from the Network of Excellence IDECAT (NMP3-CT-2005-011730, Integrated Design of Catalytic Nanomaterials for a Sustainable Production) granted by the European Commission and from the "Région Rhône-Alpes" is gratefully acknowledged.

Supporting Information Available: Simulated IR spectra for $Cp_2Cr(CO)$, $[CpCr(CO)_3]^-$, and $[Cp_2Cr(CO)]^+$ species as obtained by adopting the hybrid DFT B3LYP functional. This material is available free of charge via the Internet at http://pubs.acs.org.

References and Notes

(1) Ozin, G. A.; Gil, C. *Chem. Rev.* **1989**, *89*, 1749–1764.
(2) Stucky, G. D.; Macdougall, J. E. *Science* **1990**, *247*, 669–678.
(3) Sachtler, W. M. H.; Zhang, Z. C. *Adv. Catal.* **1993**, *39*, 129–220.
(4) Davis, M. E. *Nature* **2002**, *417*, 813–821.
(5) Kemner, E.; Overweg, A. R.; van Eijck, L.; Fitch, A. N.; Suard, E.; de Schepper, I. M.; Kearley, G. J. *J. Chem. Phys.* **2002**, *116*, 10838–10845.
(6) Kaiser, C. T.; Gubbens, P. C. M.; Kemner, E.; Overweg, A. R.; Jayasooriya, U. A.; Cottrell, S. P. *Chem. Phys. Lett.* **2003**, *381*, 292–297.
(7) Long, J. L.; Wang, X. X.; Zhang, G. Y.; Dong, J. G.; Yan, T. J.; Li, Z. H.; Fu, X. Z. *Chem.—Eur. J.* **2007**, *13*, 7890–7899.
(8) Coperet, C.; Chabanas, M.; Saint-Arroman, R. P.; Basset, J. M. *Angew. Chem., Int. Ed.* **2003**, *42*, 156–181, and references therein.
(9) De Vos, D. E.; Sels, B. F.; Jacobs, P. A. *Adv. Catal.* **2002**, *46*, 1–87.
(10) Mesu, J. G.; Visser, T.; Beale, A. M.; Soulimani, F.; Weckhuysen, B. M. *Chem.—Eur. J.* **2006**, *12*, 7167–7177.
(11) Kervinen, K.; Bruijnincx, P. C. A.; Beale, A. M.; Mesu, J. G.; van Koten, G.; Gebbink, R.; Weckhuysen, B. M. *J. Am. Chem. Soc.* **2006**, *128*, 3208–3217.
(12) Corma, A.; Garcia, H. *Eur. J. Inorg. Chem.* **2004**, 1143–1164.
(13) Alvaro, M.; Chretien, M. N.; Ferrer, B.; Fornes, V.; Garcia, H.; Scaiano, J. C. *Chem. Commun.* **2001**, 2106–2107.
(14) Weber, W. A.; Phillips, B. L.; Gates, B. C. *Chem.—Eur. J.* **1999**, *5*, 2899–2913.
(15) Zhan, B. Z.; Li, X. Y. *Chem. Commun.* **1998**, 349–350.
(16) Cano, M. L.; Corma, A.; Fornes, V.; Garcia, H.; Miranda, M. A.; Baerlocher, C.; Lengauer, C. *J. Am. Chem. Soc.* **1996**, *118*, 11006–11013.
(17) Corma, A.; Fornes, V.; Garcia, H.; Miranda, M. A.; Primo, J.; Sabater, M. J. *J. Am. Chem. Soc.* **1994**, *116*, 2276–2280.
(18) Ozin, G. A.; Godber, J. *J. Phys. Chem.* **1989**, *93*, 878–893.
(19) Davis, R.; Kane-Maguire, L. A. P. In *Comprehensive Organometallic Chemistry*; Wilkinson, G., Stone, F. G. A., Abel, E. W., Eds.; Pergamon: Oxford, U.K., 1982; Vol. 3,Chapters 27.2 and 28.2.
(20) Morris, M. J. *Comprehensive Organometallic Chemistry*; Wilkinson, G., Stone, F. G. A., Abel, E. W., Eds.; Pergamon: Oxford, U.K., 1992; Vol. 5,Chapter 7.
(21) Brintzinger, H. H.; Fischer, D.; Mulhaupt, R.; Rieger, B.; Waymouth, R. M. *Angew. Chem., Int. Ed.* **1995**, *34*, 1143–1170.
(22) Alt, H. G.; Koppl, A. *Chem. Rev.* **2000**, *100*, 1205–1221, and references therein.
(23) Kaminsky, W.; Laban, A. *Appl. Catal., A* **2001**, *222*, 47–61.
(24) Zhang, J.; Wang, X.; Jin, G. X. *Coord. Chem. Rev.* **2006**, *250*, 95–109.
(25) Karol, F. J.; Brown, G. L.; Davison, J. M. *J. Polym. Sci., Part A* **1973**, *11*, 413–424.
(26) Karol, F. J.; Wu, C. *J. Polym. Sci., Part A* **1974**, *12*, 1549–1558.
(27) Tang Wong, K. L.; Brintzinger, H. H. *J. Am. Chem. Soc.* **1975**, *97*, 5143–5146.
(28) Brintzinger, H. H.; Lohr, L. L. J.; Tang Wong, K. L. *J. Am. Chem. Soc.* **1975**, *97*, 5146–5155.
(29) Sneeden, R. P. A. *Organochromium Compounds*; Academic Press: New York, 1975.
(30) Estephane, J.; Groppo, E.; Vitillo, J. G.; Damin, A.; Lamberti, C.; Bordiga, S.; Zecchina, A. *Phys. Chem. Chem. Phys.* 2009, *11*, 2218−2227.
(31) Lamberti, C.; Bordiga, S.; Geobaldo, F.; Zecchina, A.; Otero Arean, C. *J. Chem. Phys.* **1995**, *103*, 3158–3165.
(32) Zecchina, A.; Bordiga, S.; Lamberti, C.; Spoto, G.; Carnelli, L.; Otero Arean, C. *J. Phys. Chem.* **1994**, *98*, 9577–9582.
(33) Zecchina, A.; Spoto, G.; Bordiga, S. *Faraday Discuss. Chem. Soc.* **1989**, *87*, 149–160.
(34) Lamberti, C.; Bordiga, S.; Bonino, F.; Prestipino, C.; Berlier, G.; Capello, L.; D'Acapito, F.; Llabres i Xamena, F. X.; Zecchina, A. *Phys. Chem. Chem. Phys.* **2003**, *5*, 4502–4509.
(35) Turnes Palomino, G.; Bordiga, S.; Zecchina, A.; Marra, G. L.; Lamberti, C. *J. Phys. Chem. B* **2000**, *104*, 8641–8651.
(36) Lamberti, C.; Bordiga, S.; Arduino, D.; Zecchina, A.; Geobaldo, F.; Spanò, G.; Genoni, F.; Petrini, G.; Carati, A.; Villain, F.; Vlaic, G. *J. Phys. Chem. B* **1998**, *102*, 6382–6390.
(37) Frisch, M. J.; Trucks, G. W.; Schlegel, H. B.; Scuseria, G. E.; Robb, M. A.; Cheeseman, J. R.; Montgomery, J. A., Jr.; Vreven, T.; Kudin, K. N.; Burant, J. C.; Millam, J. M.; Iyengar, S. S.; Tomasi, J.; Barone, V.; Mennucci, B.; Cossi, M.; Scalmani, G.; Rega, N.; Petersson, G. A.; Nakatsuji, H.; Hada, M.; Ehara, M.; Toyota, K.; Fukuda, R.; Hasegawa, J.; Ishida, M.; Nakajima, T.; Honda, Y.; Kitao, O.; Nakai, H.; Klene, M.; Li, X.; Knox, J. E.; Hratchian, H. P.; Cross, J. B.; Bakken, V.; Adamo, C.; Jaramillo, J.; Gomperts, R.; Stratmann, R. E.; Yazyev, O.; Austin, A. J.; Cammi, R.; Pomelli, C.; Ochterski, J. W.; Ayala, P. Y.; Morokuma, K.; Voth, G. A.; Salvador, P.; Dannenberg, J. J.; Zakrzewski, V. G.; Dapprich, S.; Daniels, A. D.; Strain, M. C.; Farkas, O.; Malick, D. K.; Rabuck, A. D.; Raghavachari, K.; Foresman, J. B.; Ortiz, J. V.; Cui, Q.; Baboul, A. G.; Clifford, S.; Cioslowski, J.; Stefanov, B. B.; Liu, G.; Liashenko, A.; Piskorz, P.; Komaromi, I.; Martin, R. L.; Fox, D. J.; Keith, T.; Al-Laham, M. A.; Peng, C. Y.; Nanayakkara, A.; Challacombe, M.; Gill, P. M. W.; Johnson, B.; Chen, W.; Wong, M. W.; Gonzalez, C.; Pople, J. A. *Gaussian 03*, revision C.02; Gaussian, Inc.: Wallingford, CT, 2004.
(38) Becke, A. D. *Phys. Rev. A* **1988**, *38*, 3098–3100.
(39) Lee, E. P. F.; Wright, T. G. *Phys. Chem. Chem. Phys.* **1999**, *1*, 219–225.
(40) Schafer, A.; Huber, C.; Ahlrichs, R. *J. Chem. Phys.* **1994**, *100*, 5829–5835.
(41) Hehre, W. J.; Radom, L.; Schleyer, P. v. R.; Pople, J. A. *Ab Initio Molecular Orbital Theory*; John Wiley & Sons, Inc.: New York, 1986.
(42) Fritz, H. P.; Schwarzhans, K. E. *J. Organomet. Chem.* **1964**, *1*, 208–211.
(43) Xu, Z. F.; Xie, Y. M.; Feng, W. L.; Schaefer, H. F. *J. Phys. Chem. A* **2003**, *107*, 2716–2729.
(44) Ankudinov, A. L.; Rehr, J. J. *Phys. Rev. B* **2000**, *62*, 2437–2445.
(45) Poiarkova, A. V.; Rehr, J. J. *J. Synchrotron. Radiat.* **1999**, *6*, 313–314.
(46) Poiarkova, A. V.; Rehr, J. J. *Phys. Rev. B* **1999**, *59*, 948–957.
(47) Ravel, B.; Newville, M. *J. Synchrotron. Radiat.* **2005**, *12*, 537–541.
(48) Ankudinov, A. L.; Ravel, B.; Rehr, J. J.; Conradson, S. D. *Phys. Rev. B* **1998**, *58*, 7565–7576.
(49) Ruiz-Lopez, M. F.; Loos, M.; Goulon, J.; Benfatto, M.; Natoli, C. R. *Chem. Phys.* **1988**, *121*, 419–437.
(50) Marra, G. L.; Fitch, A. N.; Zecchina, A.; Ricchiardi, G.; Salvalaggio, M.; Bordiga, S.; Lamberti, C. *J. Phys. Chem. B* **1997**, *101*, 10653–10660.
(51) Haaland, A. *Top. Curr. Chem.* **1975**, *53*, 1.
(52) Gordon, K. R.; Warren, K. D. *Inorg. Chem.* **1978**, *17*, 987–994.
(53) Warren, K. D. *Struct. Bonding (Berlin, Ger.)* **1976**, *27*, 46.
(54) Yamaguchi, Y.; Ding, W.; Sanderson, C. T.; Borden, M. L.; Morgan, M. J.; Kutal, C. *Coord. Chem. Rev.* **2007**, *251*, 515–524.
(55) Note that the scheme is not strictly rigorous. Electronic transitions should be expressed in terms of group theory, once all the possible excited configurations have been taken into account. Arrows representing bands I, II, and III have to be considered only as a simplified way to illustrate which electron is undergoing a transition and toward which type of molecular orbital. Notwithstanding the lack of a rigorous language, Figure 2b has the advantage to show, in an easy way and with a single scheme, the origin of the optical absorptions and XANES features of Cp_2Cr molecules. This scheme represents one of the few attempts in the literature to match the information obtained with these two techniques.
(56) Muraoka, P. T.; Byun, D.; Zink, J. I. *J. Phys. Chem. A* **2001**, *105*, 8665–8671.
(57) Warren, K. D. *Inorg. Chem.* **1974**, *13*, 1243–1246.
(58) Brennan, J.; Cooper, G.; Green, J. C.; Payne, M. P.; Redfern, C. M. *J. Electron Spectrosc. Relat. Phenom.* **1993**, *66*, 101–115.
(59) Chetwynd-Talbot, J.; Grebenik, P.; Perutz, R. N. *Inorg. Chem.* **1982**, *21*, 3641–3651.

(60) Kolczewski, C.; Hermann, K. *Theor. Chem. Acc.* **2005**, *114*, 60–67.

(61) Tromp, M.; Moulin, J. O.; Reid, G.; Evans, J. *AIP Conf. Proc.* **2007**, *882*, 699–701.

(62) Moulin, J. O.; Evans, J.; McGuinness, D. S.; Reid, G.; Rucklidge, A. J.; Tooze, R. P.; Tromp, M. *Dalton Trans.* **2008**, 1177–1185.

(63) Aleksanyan, V. T.; Lokshin, B. V.; Borisov, G. K.; Devyatykh, G. G.; Smirnov, A. S.; Nazarova, R. V.; Koningstein, J. A.; Gächter, B. F. *J. Organomet. Chem.* **1977**, *124*, 293–298.

(64) Parameswaran, T.; Koningstein, J. A.; Haley, L. V.; Aleksanyan, V. T. *J. Chem. Phys.* **1978**, *68*, 1285–1291.

(65) Aleksanyan, V. T.; Greenwald, I. I. *J. Mol. Struct.* **1982**, *90*, 35–47.

(66) Khodakov, A. Y.; Kustov, L. M.; Kazansky, V. B.; Williams, C. *J. Chem. Soc., Faraday Trans.* **1992**, *88*, 3251–3253.

(67) O'Callaghan, K. A. E.; Brown, S. J.; Page, J. A.; Baird, M. C. *Organometallics* **1991**, *10*, 3119–3122.

(68) Cationic $[CpCr(CO)_3]^+$ species show much higher μ(CO) values. $[CpCr(CO)_3]^+I^-$ in toluene exhibits bands at 2030, 1974, and 1951 cm^{-1}, while $[CpCr(CO)_3]^+Br^-$ in toluene gives absorption at 2043, 1989, and 1960 cm^{-1} (Huber, T. A.; Macartney, D. H.; Baird, M. C. *Organometallics* **1995**, *14*, 592).

(69) Foo, D. M. J.; Sinnema, P. J.; Twamley, B.; Shapiro, P. J. *Organometallics* **2002**, *21*, 1005–1007.

(70) Zecchina, A.; Scarano, D.; Bordiga, S.; Spoto, G.; Lamberti, C. *Adv. Catal.* **2001**, *46*, 265–397, and references therein.

(71) Zecchina, A.; Marchese, L.; Bordiga, S.; Paze, C.; Gianotti, E. *J. Phys. Chem. B* **1997**, *101*, 10128–10135.

(72) Bordiga, S.; Damin, A.; Bonino, F.; Zecchina, A.; Spano, G.; Rivetti, F.; Bolis, V.; Prestipino, C.; Lamberti, C. *J. Phys. Chem. B* **2002**, *106*, 9892–9905.

(73) Darensbourg, M. Y.; Jimenez, P.; Sackett, J. R.; Hanckel, J. M.; Kump, R. L. *J. Am. Chem. Soc.* **1982**, *104*, 1521–1530.

(74) Longato, B.; Martin, B. D.; Norton, J. R.; Anderson, O. P. *Inorg. Chem.* **1985**, *24*, 1389–1394.

(75) Rao, K. M.; Spoto, G.; Guglielminotti, E.; Zecchina, A. *J. Chem. Soc., Faraday Trans.* **1984**, *88*, 2195–2207.

(76) Zecchina, A.; Spoto, G.; Garrone, E.; Bossi, A. *J. Phys. Chem.* **1984**, *88*, 2587–2591.

(77) In cases where the structural model to be used in an EXAFS fit is not defined, it is worth trying the different possible candidates by comparing experimental datum with simulations obtained from the models, before optimizing any structural parameters. This allows verification of whether a given model can account for all experimental features.

(78) A similar spectrum is obtained by simulating the neutral $Cp_2Cr(CO)$ adduct because its geometry is indistinguishable from that of the cation within the EXAFS sensitivity.

(79) Prestipino, C.; Bordiga, S.; Lamberti, C.; Vidotto, S.; Garilli, M.; Cremaschi, B.; Marsella, A.; Leofanti, G.; Fisicaro, P.; Spoto, G.; Zecchina, A. *J. Phys. Chem. B* **2003**, *107*, 5022–5030.

(80) Groppo, E.; Prestipino, C.; Cesano, F.; Bonino, F.; Bordiga, S.; Lamberti, C.; Thüne, P. C.; Niemantsverdriet, J. W.; Zecchina, A. *J. Catal.* **2005**, *230*, 98–108.

(81) Use of the same Δd_{Cr-Cp} and Δd_{Cr-CO} parameters for the $[CpCr(CO)_3]^-$ and $[Cp_2Cr(CO)]^+$ phases is justified because, within the experimental errors, the same Δd_{Cr-Cp} and Δd_{Cr-CO} parameters have been obtained in the two fits performed with a single phase (see fourth and fifth columns in Table 3).

(82) The most relevant correlations are $\sigma^2_{Cr-Cp}/x = -0.81$, $\sigma^2_{Cr-CO}/x = +0.80$, $\Delta E_0/\Delta d_{Cr-Cp} = 0.77$, and $\sigma^2_{Cr-Cp}/\sigma^2_{Cr-CO} = -0.75$; all remaining correlations are lower than 0.6 in absolute value.

(83) van Raaij, E. U.; Brintzinger, H. H. *J. Organomet. Chem.* **1988**, *356*, 315–323.

(84) Overweg, A. R.; Koller, H.; de Haan, J. W.; van de Ven, L. J. M.; van der Kraan, A. M.; van Santen, R. A. *J. Phys. Chem. B* **1999**, *103*, 4298–4308.

(85) Vitale, G.; Mellot, C. F.; Bull, L. M.; Cheetham, A. K. *J. Phys. Chem. B* **1997**, *101*, 4559–4564.

(86) Garcia, H.; Roth, H. D. *Chem. Rev.* **2002**, *102*, 3947–4007.

(87) Astruc, D. *Electron Transfer and Radical Processes in Transition Metal Chemistry*; Wiley-VCH: New York, 1995.

JP811240M